



1 **Evaluating low-cost NDIR CO₂ for atmospheric**
2 **observation in rural settings**

3 Olalekan A.M. Popoola*¹, Paolo Cicuta¹, Rachel H. Georgiou¹, Lawrence Tom¹, Ray
4 Freshwater¹, Kelsey Leet¹, Chiara Giorio*¹

5 ¹Yusuf Hamied Department of Chemistry, University of Cambridge, Cambridge, CB2 1EW,
6 United Kingdom.

7

8 *Correspondence to: Olalekan Popoola (oamp2@cam.ac.uk) and Chiara Giorio
9 (chiara.giorio@atm.ch.cam.ac.uk)

10 **Abstract**

11 Most research and monitoring activities involving low-cost atmospheric sensors (LCS) have
12 traditionally focused on urban environments, where air quality is a pressing concern. However,
13 an emerging area of research is their application in rural landscapes, where land use is a key
14 determinant of climate change and net zero outcomes, directly influencing greenhouse gas
15 emissions, carbon sequestration, and ecosystem functioning. In this study, we examine the
16 use of LCS NDIR CO₂ sensors to monitor atmospheric concentrations in agricultural settings.
17 We present a data analysis framework that addresses errors associated with factory auto-
18 baseline correction and, crucially, accounts for the influence of environmental parameters such
19 as temperature and pressure. This approach leads to improved sensor performance. Results
20 from deployments in both rural and urban environments demonstrate strong agreement with
21 reference-grade instruments, as shown by the root mean square error (RMSE) and coefficient
22 of determination (R^2). Improvements of RMSE from 10 ppm to 4 ppm in winter and 5 ppm to
23 4 ppm in summer, with corresponding improved R^2 from 0.85 to 0.98 in winter and 0.86 to 0.97
24 in summer were obtained when compared to a simple scaling correction of the out-of-box data.
25 Our study shows that corrected data not only reproduced the seasonal profile associated with
26 rural emissions, but it also captured the diurnal variability, sometimes characterised by CO₂
27 change of up to 50 ppm, which is more than three times (15 ppm) the typical change in the
28 urban environment. Overall, this study demonstrates the viability of low-cost CO₂ sensors and
29 sensor networks for reliable long-term monitoring in rural environments. The observations
30 obtained provide valuable inputs for developing analytical methodologies and offer actionable
31 insights into the influence of rural land-use practices on climate.

32



33 **1. Introduction**

34 Carbon dioxide (CO₂) is a greenhouse gas that drives the warming of Earth's climate. The
35 United Nations Sustainable Development Goals and the Intergovernmental Panel on Climate
36 Change (IPCC) state that CO₂ emissions must be drastically reduced by 2030 to prevent
37 atmospheric warming above 1.5 °C (IPCC, 2018). This goal requires both international
38 collaboration and effective monitoring technologies to collectively reduce carbon emissions.
39 CO₂ measurements can be used to estimate emission rates (Martin et al., 2017) but have
40 historically been limited by the high cost of necessary instrumentation.

41 In recent years, technological advancements in low-cost sensors (LCS) have enabled wider
42 air quality monitoring and are increasingly being applied to greenhouse gas observations
43 (Dubey et al., 2024). The availability of these relatively inexpensive CO₂ detectors (costing in
44 the range of hundreds of dollars) has facilitated their integration into multispecies sensor
45 platforms for network deployments of low-cost monitoring devices (Turner et al., 2016; Wu et
46 al., 2016; Lopez-Coto et al., 2017). They commonly utilise a non-dispersive infrared (NDIR)
47 detector and are typically small, portable, and require little power. These characteristics allow
48 for the sensors' incorporation in diverse environments, as they do not require pre-existing
49 infrastructure or costly installation campaigns.

50 Low-cost sensors expand access to reliable field-scale environmental data and increase the
51 spatial coverage and resolution of CO₂ measurements (Martin et al., 2017). These sensors
52 enable the deployment of affordable monitoring networks capable of quantifying whole-site
53 emissions, seasonal variability, and crop-specific differences in CO₂ fluxes (Miles et al., 2021;
54 Yang et al., 2021). By lowering financial and technical barriers, these systems extend access
55 to actionable CO₂ data in rural, resource-limited regions, supporting emissions assessment,
56 land-management decisions, and public health planning (Wu et al., 2016; Turner et al., 2016).
57 These sensors also empower sustainable agriculture initiatives by enabling farmers to monitor
58 carbon outputs at the field scale and assess crop-specific emissions, seasonal variability, and
59 machinery-related contributions (Martin et al., 2017; Müller et al., 2020). In rural settings, CO₂
60 emissions are largely influenced by land use, which may range from agricultural activities (both
61 arable and pastoral) to natural reserves, leading to spatial and temporal variation in emission
62 profiles (Miles et al., 2021). In arable farming regions, CO₂ exchange is driven by daytime
63 photosynthesis during the growing season and by soil and ecosystem respiration after harvest
64 (Miles et al., 2021). Quantifying these fluxes at local scales typically relies on eddy covariance
65 flux systems, which directly measure the net exchange of CO₂ between the land surface and
66 the atmosphere but can be financially prohibitive for many research or management
67 applications (Wu et al., 2016). Low-cost CO₂ sensors offer a potential solution to this challenge



68 by enabling network-based deployments that, when integrated with atmospheric models, allow
69 for enhanced field-scale emission estimation (Martin et al., 2017; Turner et al., 2016).
70 However, the effectiveness of this approach relies on the availability of robust, high spatio-
71 temporal datasets that accurately capture environmental and management influences on CO₂
72 dynamics. Previous studies have successfully deployed these sensors in urban environments
73 for applications such as source identification and data assimilation into atmospheric models,
74 supporting emission inventory assessments and source footprint evaluations (Delaria et al.,
75 2021; Dubey et al., 2024; Shusterman et al., 2018). Another study evaluated several LCS
76 brands against a reference analyser in an urban environment to verify measurement
77 performance (Cai et al., 2025). However, the use of LCS for CO₂ monitoring in rural
78 environments remains limited. Macagga et al. (2024) deployed these sensors in rural
79 environments alongside higher-end reference instrumentation to assess ecosystem carbon
80 balance and other studies have utilised low-cost sensors as components of larger devices for
81 *in situ* soil carbon measurements (Heger et al., 2020) or chamber-based systems for citizen
82 science projects (Sloan et al., 2025). We aim to build on these rural applications through the
83 development of a rigorous, cross-site data-processing protocol that accounts for sensor drift
84 over time, seasonal variability, and differences in temperature and humidity (Cai et al., 2025).

85 In this study, we evaluate the performance of a set of low-cost CO₂ sensors in both rural and
86 urban environments. Specifically, we examine methods for improving raw factory-calibrated
87 data by accounting for environmental influences and implementing best practices for quality
88 assurance and quality control (QA/QC) to enhance data accuracy across sites.

89 **2. Methodology**

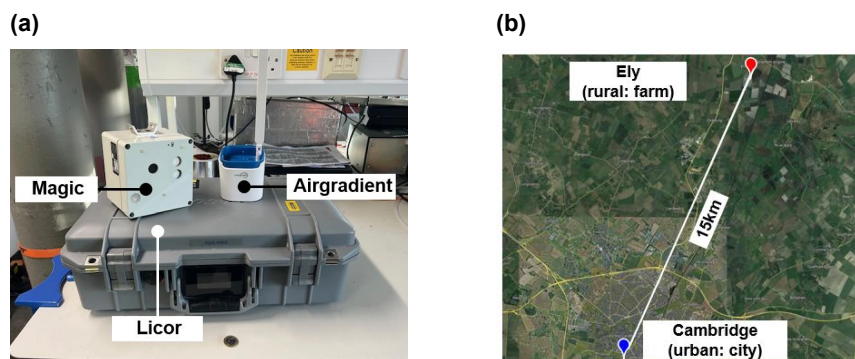
90 **2.1 Study Locations**

91 This study was conducted at two sites (one rural and one urban) to assess the potential of
92 LCS CO₂ sensors in rural environments. The rural site was an arable farm in Stretham, near
93 Ely, UK, where LCS CO₂ nodes were deployed alongside a reference-grade CO₂ analyser at
94 a height of 1.5 m.

95 A similar monitoring setup was established at the urban site, located approximately 16 km
96 away in Cambridge. The urban measurements were conducted on the rooftop of the Yusuf
97 Hamied Department of Chemistry, University of Cambridge (52°11'52.64"N, 0°7'29.92"E) at
98 an approximate height of 22 m. The study locations are shown in Figure 1.

99

100



101

102 **Figure 1: Instrumentation and study sites. (a) LCS CO₂ devices (Magic and AirGradient**
103 **nodes) and the reference LI-COR CO₂ analyser. (b) Map showing the locations of the**
104 **rural and urban study sites. Background imagery in (b) from Google Earth Pro (Imagery**
105 **©2026 Google; map data ©2026 Google).**

106 2.2 Meteorological data and statistical analysis

107 The performance of the LCS data was assessed against the reference measurements using
108 a range of statistical indicators, including root mean square error (RMSE), mean absolute error
109 (MAE), coefficient of determination (R^2), and the slope and intercept of a least-squares linear
110 regression fit. Overall results were consolidated using a Taylor diagram, a two-dimensional
111 statistical visualisation that combines three key metrics: standard deviation (SD), Pearson's
112 correlation coefficient (r), and centred root mean square error (cRMSE), which corresponds to
113 the RMSE of bias-corrected data. This was implemented using the openair package in R
114 (Carslaw, 2012).

115 Supporting meteorological data for London Heathrow airport, 51°28'39.0"N 0°27'41.0"W and
116 Lakenheath airport, 52°25'12.0"N 0°34'00.0"E were obtained from the National Oceanic and
117 Atmospheric Administration (NOAA) Integrated Surface Database (ISD) using the R worldmet
118 package (Carslaw, 2020).

119 2.3 Low-Cost CO₂ Sensor Nodes

120 A bespoke portable monitoring system, known as the "Magic Box", was initially utilised for CO₂
121 and air quality measurements at both study locations. This device has been successfully used
122 in previous air quality studies in urban environments (Song et al., 2018). CO₂ was monitored
123 using the original equipment manufacturer (OEM) device Senseair K33 sensor (Senseair, K33,
124 2025), which operates on NDIR technology. The Automatic Baseline Correction (ABC) default
125 setting in the K33 had been turned off, thus limiting error associated with ABC (section 2.4.2).



126 A pair of the Magic boxes was collocated outdoors with a reference CO₂ monitor for a period
127 of 12 days at the urban site (7 to 18 December 2022), nodes were then deployed at the rural
128 site between 20 December and 22 January 2023 (~1 month) in close proximity to a rural
129 reference monitor (< 200 m). The out-of-the-box CO₂ data were calibrated to the reference
130 data obtained from the reference LI-COR CO₂ instrument using a 2-day period (14-15
131 December 2022) during the 12-day initial collocation at the urban site.

132 The results (see section 3.5) from those initial deployments informed the decision to
133 incorporate an additional portable CO₂ monitoring sensor system, the AirGradient Open Air
134 outdoor air quality monitor. This device measures particulate matter (PM), total volatile organic
135 compounds (TVOCs), CO₂, temperature, and relative humidity. The selection of this alternative
136 LCS device was motivated by the improved design of its weatherproof housing, which
137 incorporates mesh openings that allow enhanced air exchange relative to the Magic box. This
138 design reduces the likelihood of air stagnation within the enclosure and minimises internal
139 humidity variability in response to changes in external environmental conditions. CO₂
140 concentrations were specifically measured using the Senseair S8 NDIR sensor (Senseair, S8,
141 2025). Unlike the Magic devices, the ABC setting in the AirGradient with the S8 sensor was
142 active by default when the AirGradient units were sourced. We also assessed the viability of
143 Senseair Sunrise sensors for rural application using a version of AirGradient that incorporated
144 Sunrise CO₂ sensor (with the ABC off) as the main CO₂ detector. To evaluate the network
145 applicability of LCS CO₂ in rural settings, we deployed a network (four nodes) made up of
146 slightly modified AirGradient Open Air outdoor that used Senseair Sunrise CO₂ OEM device
147 (Senseair, Sunrise, 2025). This modification to the CO₂ detector in the AirGradient was
148 informed by the need to reduce power demand in the sensor system, S8 average current is
149 orders of magnitude higher than Sunrise (18 mA compared to 1-34 μ A). Although the CO₂
150 detectors used in the LCS devices in this study were all sourced from the same manufacturer,
151 the analytical approach and recommendations for improved performance are generalisable
152 and can be applied to other NDIR or LCS CO₂ sensors.

153 For the purposes of this study, we focus exclusively on CO₂ measurements from these sensor
154 deployments, and not on the other measured parameters by the same sensor platforms. We
155 used LI-COR LI-7815 CO₂/H₂O instrument co-located in the same environment as our
156 reference grade analyser. It is based on an Optical Feedback-Cavity Enhanced Absorption
157 Spectroscopy (OF-CEAS), with a 100 ppb resolution at 1 s averaging and response time less
158 than 2 seconds (LI-COR, 2025). The reference data were averaged to 5-minute resolution to
159 match the sampling rate of the AirGradient LCS CO₂ used in this study. Figure 1 (a) shows an
160 image of the different instrumentations and Table 1 summarises the information for the various
161 sensor platform, deployment type and duration of monitoring for our study.



162 **Table 1. Summary of the sensor system, CO₂ type and configuration, form and duration**
163 **of deployment of study.**

Sensor system	OEM CO ₂	ABC Active	Deployment period	Deployment type
Magic	K33	No	December 2022-Jan 2023	Collocation (urban and rural)
AirGradient	S8	Yes	May 2023-February 2025	Collocation (urban and rural)
AirGradient	Sunrise	No	August-September 2024	Network (rural)

164

165 **2.4 Sources of errors in LCS NDIR CO₂**

166 **2.4.1 Effect of OEM Automatic Baseline Correction (ABC) on CO₂ signal**

167 Automatic Baseline Correction (ABC) is a CO₂ signal processing feature available as part of
168 the NDIR CO₂ sensors employed in this study. Initially, the sensor manufacturer recommended
169 enabling this function, as it is intended to correct for baseline drift over time. The ABC algorithm
170 is activated when the measured CO₂ baseline falls below the background concentration,
171 typically set by default at 400 ppm. The system periodically assesses whether this condition
172 has been met over a predefined interval, usually ten days, although this period may vary. If
173 the sensor records CO₂ concentrations below 400 ppm for the majority of that interval, the
174 algorithm calculates the deviation and applies an automatic correction to the baseline.

175 Whilst we did not observe baseline drift in our study when the ABC was deactivated, long-term
176 drift is expected to introduce error into the measurements. Users should therefore characterise
177 this drift by detrending the data prior to applying the environmental correction framework
178 (section 3.3) presented in this work.

179 **2.4.2 Effect of external environmental factors on LCS CO₂ signal**

180 Previous studies have demonstrated that LCS used for the measurement of other atmospheric
181 species are influenced by environmental parameters, particularly temperature (Crilley et al.,
182 2018; Di Antonio et al., 2018; Mead et al., 2013; Spinelle et al., 2017). These effects are often
183 attributable to inherent trade-offs between portability and cost on the one hand, and instrument
184 sensitivity and measurement resolution on the other. Another factor that suggests the possible
185 effect of external environmental parameters on the performance of LCS under real world
186 application is the fact that they are often calibrated under controlled environmental conditions
187 in the lab. NDIR is a spectroscopic technique, and any external factors that might affect its
188 optics and detectors will impact sensor performance. The extreme temperature diurnal
189 variabilities characteristic of summertime might affect the optics and invariably sensor
190 performance. On an extended timescale, we postulate that pressure could additionally affect



191 the performance of the CO₂ sensor. The provenance of this effect can be related to the fact
 192 that the sensors OEM are calibrated at a fixed pressure and report the signal in mixing ratios
 193 (parts per million, ppm) denoted by symbol χ in Eq. (1). Number density (n) of atmospheric
 194 gas species varies with pressure as shown in the relationship in Eq. (1), since the LCS CO₂
 195 uses information from a fixed laboratory pressure calibration (P_{lab}), a changing ambient
 196 pressure ($P_{atmosphere}$) would be expected to impact the sensor.

$$197 \quad \chi_{species} = \frac{n_{species}}{n_{atmosphere}} = \frac{\left(\frac{N_{species}}{V_{atmosphere}}\right)}{\left(\frac{N_{atmosphere}}{V_{atmosphere}}\right)} = \frac{\left(\frac{N_{species}}{V_{atmosphere}}\right)}{\left(\frac{P_{atmosphere}}{kT}\right)} \quad (1)$$

198 Where $\chi_{species}$ represents mixing ratio of the monitored species, $N_{species}$ and $N_{ambient}$ indicates
 199 the number of moles of the species and ambient respectively, V is the volume, k Boltzmann's
 200 constant and T the absolute temperature. It follows that the ratio of the mixing ratios expression
 201 from Eq. (1), for a LCS calibrated at a fixed lab pressure of (P_{fixed}) relative to a reference device
 202 which has pressure compensation, is given by the expression in Eq. (2).

$$203 \quad \frac{\chi_{species}^{LCS}}{\chi_{species}^{reference}} = \frac{\left(\frac{N_{species}}{V_{ambient}}\right)}{\left(\frac{P_{fixed}}{kT}\right)} * \left[\frac{\left(\frac{N_{species}}{V_{ambient}}\right)}{\left(\frac{P_{ambient}}{kT}\right)}\right]^{-1} = \frac{P_{ambient}}{P_{fixed}} \quad (2)$$

204

$$205 \quad \chi_{species}^{LCS} = g * \left(\frac{P_{ambient}}{P_{fixed}}\right) * \chi_{species}^{reference} + offset \quad (3)$$

206 If we consider a LCS might have an *offset* and non-pressure related gain g , this expression
 207 can be simplified further to show that the final pressure dependence of the mixing ratio LCS
 208 in relation to reference device mixing ratio can be reformulated as Eq. (3). An optimised
 209 version of Eq. (3) was used to generate the pressure corrected CO₂ mixing ratio as formulated
 210 in Eq. (4), where the P_{fixed} is 1012 mBar and the $P_{ambient}$ uses the hourly pressure data
 211 described in section 2.2.

$$212 \quad \chi_{CO2}^{raw} = \left[\left(1.10348 * \left(\frac{P_{ambient}}{P_{fixed}} \right) - 0.218656 \right) * \chi_{CO2}^{Pcorr} \right] + 52 \text{ ppm} \quad (4)$$

213 For the temperature correction, we found an exponential temperature dependence correction
 214 factor for the CO₂ sensor sensitivity worked best for the Sunrise S8 sensor (Eq. (5)) and a
 215 linear temperature dependence sensitivity correction for the Senseair Sunrise detector, Eq.
 216 (6).

$$217 \quad \chi_{CO2}^{Pcorr} = [A_{S8} + (B_{S8} * C_{S8}^{sensorT})] * \chi_{CO2}^{Tcorr} \quad (5)$$

$$218 \quad \chi_{CO2}^{Pcorr} = [A_{Sunrise} + (B_{Sunrise} * sensorT)] * \chi_{CO2}^{Tcorr} \quad (6)$$



219 where $\chi_{CO_2}^{Pcorr}$ and $\chi_{CO_2}^{Tcorr}$ represents mixing ratio for the pressure corrected and temperature
220 corrected CO₂ respectively, $sensorT$ is the sensor temperature T expressed in Kelvin. The
221 optimal fit parameters for the S8 sensors used in our study were $A_{S8} = 0.962$, $B_{S8} =$
222 8.58×10^{-5} , $C_{S8} = 1.02$. Corresponding fit parameters for the CO₂ nodes used in the network
223 deployment are presented in Table S1.

224 **2.4.3 Effect of elevated RH on LCS CO₂ signal**

225 An NDIR sensor measures CO₂ concentrations by comparing two infrared (IR) signals (IR-
226 high and IR-low) from the same IR source at two distinct wavelengths, detected using a dual-
227 bandpass filter after transmission through the air sample within an optical cavity. For CO₂
228 measurements, the IR-high channel is centred at approximately 3.9-4.0 μm , where CO₂
229 exhibits negligible absorption (reference band), while the IR-low channel is centred around
230 4.26 μm , corresponding to a strong CO₂ absorption band. In the presence of CO₂, the IR-low
231 signal is attenuated, resulting in a reduced signal magnitude relative to the IR-high channel.

232 The presence of water vapour can influence the IR-low channel, as H₂O exhibits weak but
233 non-zero absorption within the 3-5 μm region, potentially leading to an overestimation of CO₂
234 concentrations in NDIR measurements. Under conditions of extremely high relative humidity,
235 condensation may occur on the optical cavity mirrors, causing additional signal attenuation
236 and resulting in spurious CO₂ readings. The effect of RH and water condensation on the
237 performance of NDIR is a well-known phenomenon (Cai et al., 2025; Martin et al., 2017;
238 Pereira et al., 2022; Ren et al., 2025; Wu et al., 2023; Xu et al., 2024). Most LCS devices have
239 the CO₂ sensing unit housed in a weatherproof unit and tend to rely on passive sampling to
240 minimise power demand. In the absence of an internal heating system that helps reduce water
241 condensation, in combination with a preference for passive sampling in LCS (to reduce power
242 demand), there is an increased likelihood that high RH episodes would affect the CO₂
243 measurement. Such environmental conditions are more common in rural applications than in
244 urban settings, where average temperatures are relatively higher (Si et al., 2024; Weng et al.,
245 2004). We investigated the effect of RH by deploying the same pair of Magic boxes initially in
246 the urban (December 2022) and subsequently in the rural environment (January 2023).

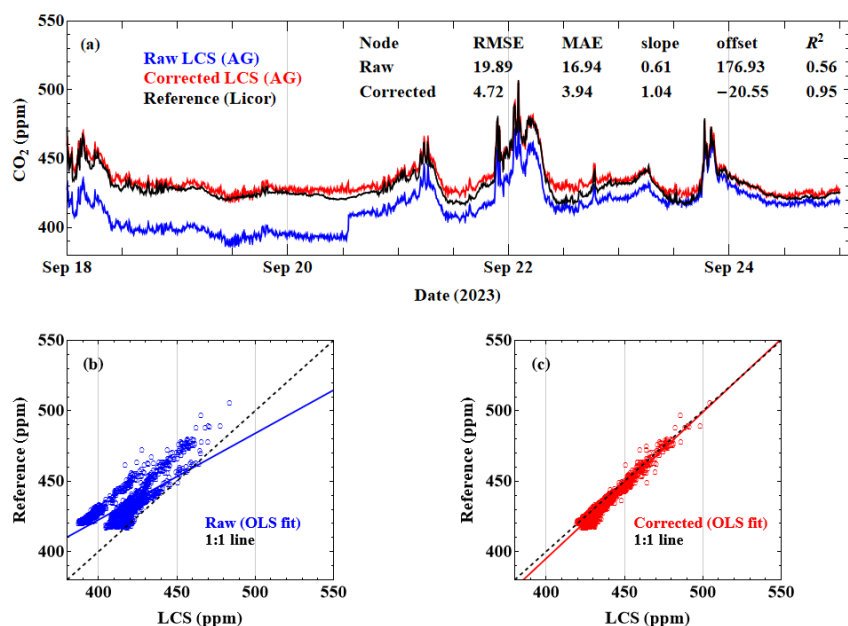
247 **3. Results and Discussion**

248 **3.1. CO₂ correction for ABC**

249 The periods during which the Automatic Baseline Correction (ABC) was triggered for the Air
250 gradient LCS CO₂ nodes used in this study were identified by examining the scatter plots from
251 collocation measurements with reference instruments at both the urban and rural sites. While
252 not all nodes exhibited a significant ABC correction, instances where this occurred were clearly



253 distinguishable as systematic errors, as illustrated in Figure 2. As expected, a significant
 254 improvement in agreement between the LCS and the reference instrument was observed
 255 when this correction was implemented (RMSE=4.7 ppm, $R^2=0.95$ compared to 19.9 ppm,
 256 $R^2=0.56$). Although this seems to suggest the only correction required is a simple ABC
 257 correction, it is worth noting that the data shown is for only a short period where the effects of
 258 environmental factors might be minimal if the meteorological conditions are ideal (minimal
 259 impact of temperature and pressure). For long-term (months) application, we evaluated the
 260 effects of environmental factors, as discussed in the next section.



261

262 **Figure 2: Comparison of LCS CO₂ against the reference. (a) Time series with associated**
 263 **validation metrics, (b) scatter plot for out-of-box LCS measurements relative to**
 264 **reference (c) scatter plot for the corrected LCS measurements (for the effect of ABC**
 265 **step) relative to reference. RMSE, slope and offset = 19.9 ppm, 0.6, 177 ppm (raw data)**
 266 **and 4.7 ppm, 1.04 and -20.6 ppm after step correction respectively.**

267 While there is merit to using the ABC method to correct potential drifts in CO₂ readings below
 268 true hemispheric background level, the method has limitations. A temporary decrease in CO₂
 269 concentration may result from environmental factors rather than true sensor drift, as will be
 270 discussed in the following section. Consequently, the automatic correction may introduce
 271 errors into the actual CO₂ measurements.

272



273 **3.2. Physical correction for the effect of environmental factors**

274 We present the results (Figure 3) of the physical correction of one of the LCS sensors deployed
275 for an extended period (a year and 7 months) from May 2023 to February 2025 in the urban
276 study location (equivalent result for the rural location shown in Figure S1). To assess the
277 performance of the data correction protocol, results from simple linear scaling commonly used
278 to calibrate out-of-the-box measurements are also shown (Figure 4 (b)). An improvement in
279 the RMSE (5.9 ppm) was observed compared to the out-of-box (44 ppm) for the collocation
280 with the reference instrument, with a comparable improvement in the scaled correction of 8.4
281 ppm. A similar improvement was reported for the MAE (44 ppm to 4.1 ppm) and the coefficient
282 of determination R^2 (0.77 to 0.89). The R^2 is particularly important because this is invariant
283 under linear scaling (Figure 3 (a) and (b)), unlike the case with corrections that incorporate the
284 effect of environmental parameters (temperature and pressure, Figures 3 (c) and 3 (d)). An
285 improvement in both R^2 and RMSE (Figure 4 (c)) was observed when the CO_2 data were
286 corrected for pressure effects (0.85 and 11.5 ppm, respectively). A substantially better
287 performance was achieved when the combined pressure and temperature corrections were
288 applied, $R^2=0.89$, RMSE=5.9 ppm, as shown in Figure 4 (d).

289

290

291

292

293

294

295

296

297

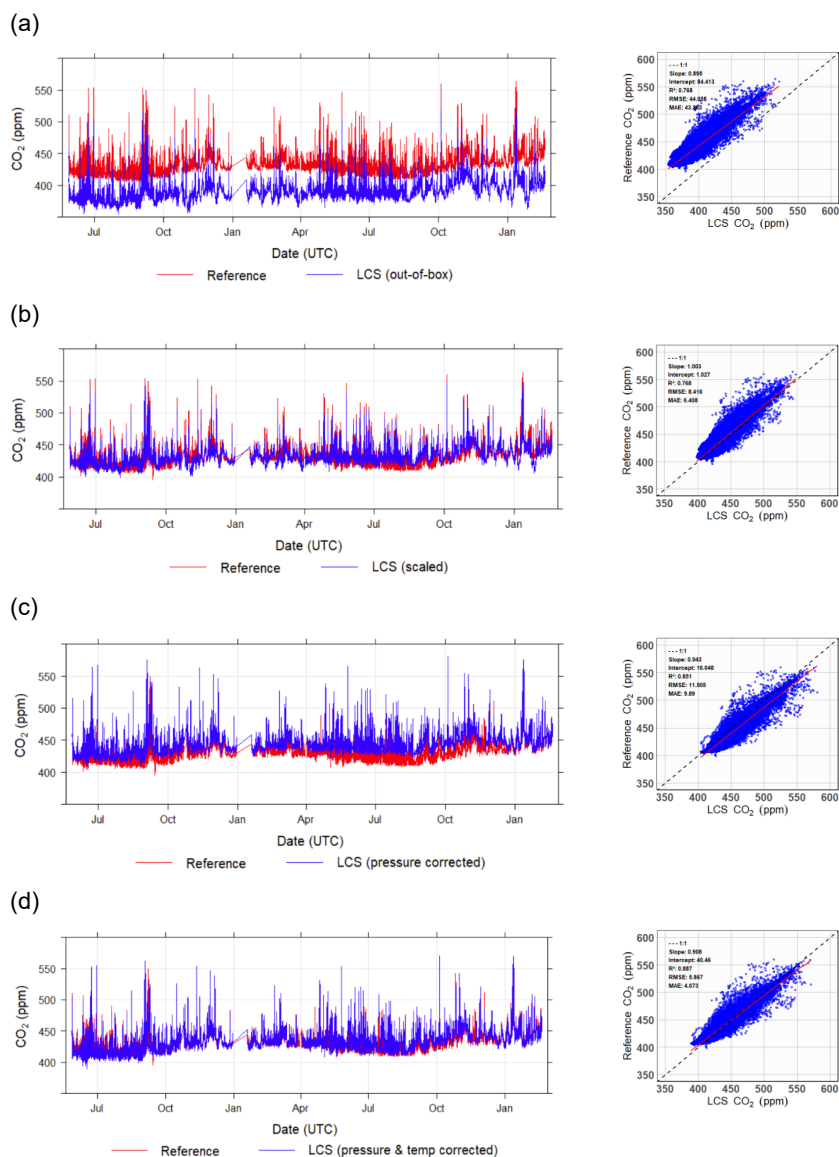
298

299

300

301

302



303 **Figure 3: Results of different calibration stages of LCS CO₂ signal for the period 22 May**
 304 **2023 to 18 February 2025 at the urban location. (a) Factory calibration, (b) simple linear**
 305 **calibration using a fixed period (1-18 August 2023), (c) pressure only correction of the**
 306 **out-of-box signal and (d) pressure and temperature correction of out-of-box signal.**

307 Figures 4 and 5 present results over a shorter period, helping to highlight the effects of
 308 pressure/temperature and how the correction improves the CO₂ performance relative to the
 309 reference. Figure 4 shows an example of a 2-month period in winter when temperature effects
 310 (mean ± SD = 4.9 ± 3.27 °C) are minimal, and the diurnal variability is small, but the pressure



311 change is significant (pressure range 970-1045 mBar, average 1018.7 ± 14.70 mBar). The
312 significant dips in the scaled LCS CO₂ readings relative to the reference before 22 December
313 2024, around 6 January and between 22 and 30 January 2025 in Figure 4 (a) coincide with
314 an ambient pressure drop from around 1020 mBar to as low as 960 mBar. The pressure-
315 temperature corrected LCS CO₂ tracks the reference data better with improved R² (0.98 vs.
316 0.85) and RMSE (4.4 ppm vs. 10.3 ppm).

317

318

319

320

321

322

323

324

325

326

327

328

329

330

331

332

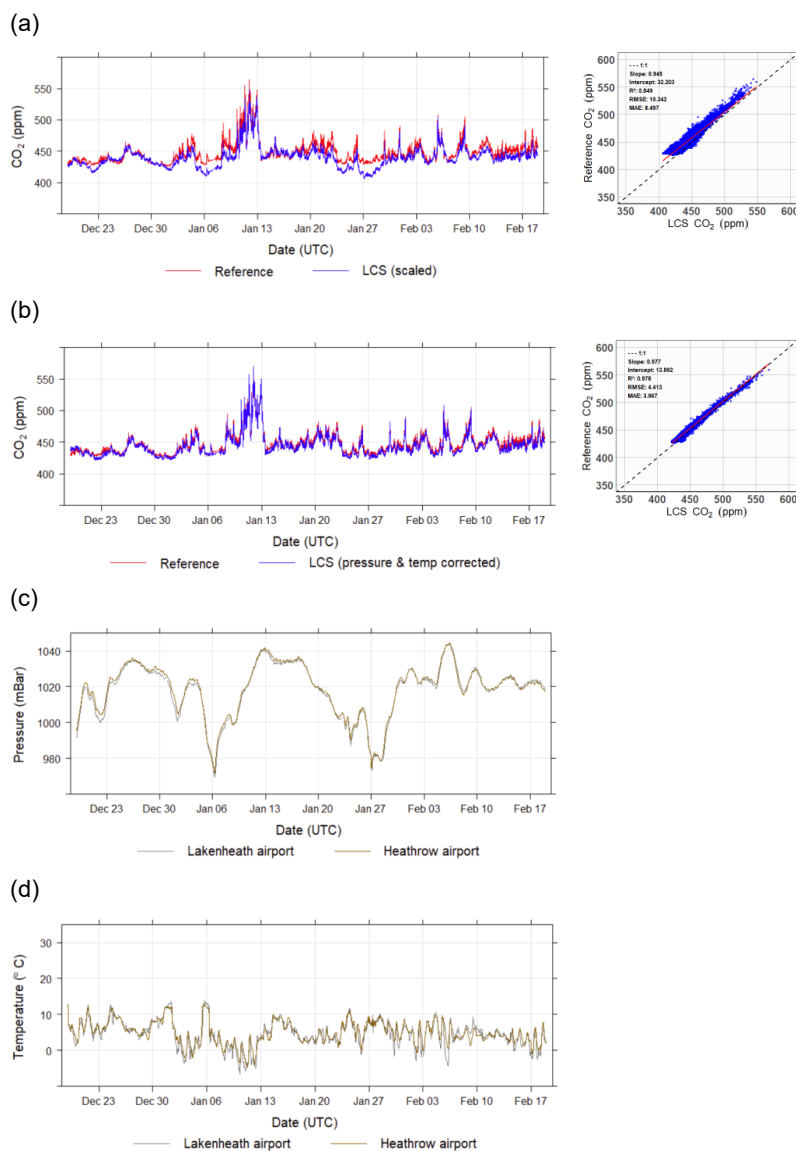
333

334

335

336

337

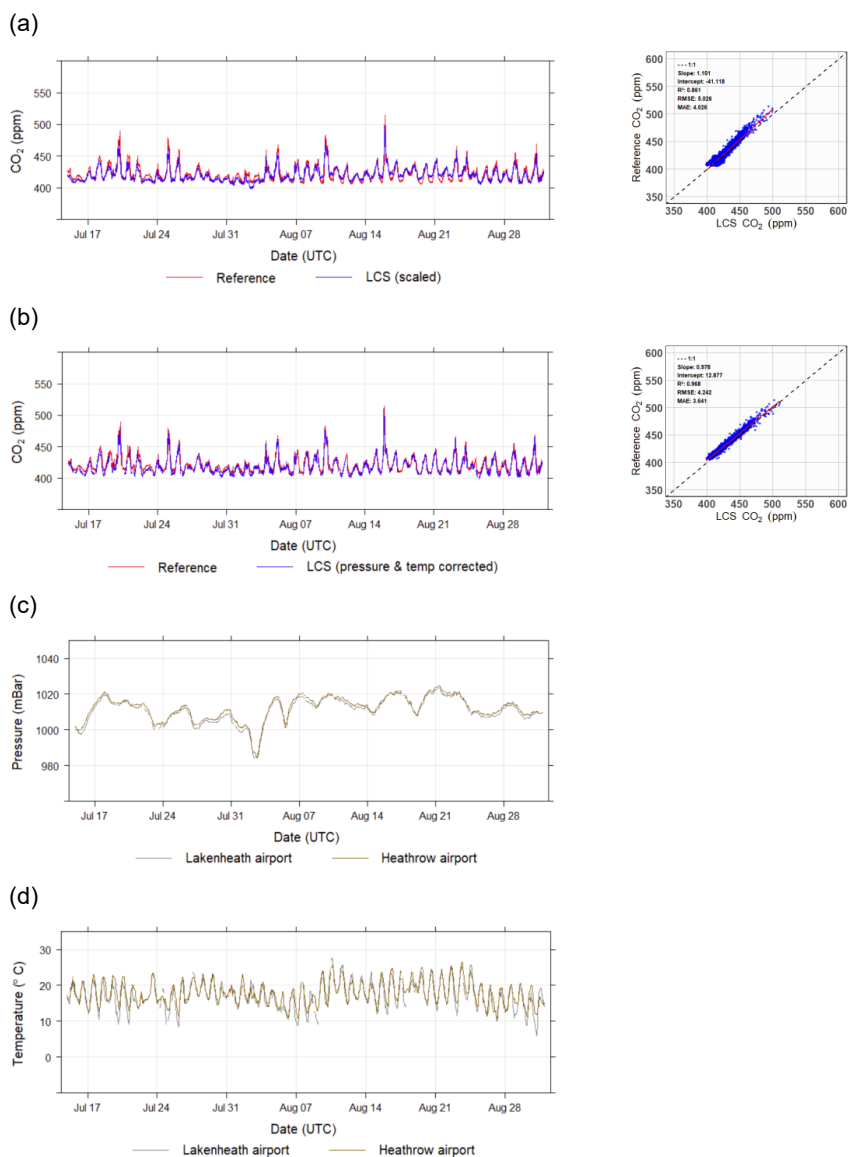


338

339 **Figure 4: Comparison of two correction methodologies for the period 19 December 2024**
340 **to 18 February 2025 at the urban location. (a) simple linear scaling correction,**
341 **(b) combined pressure-temperature corrected raw signal, (c) hourly pressure**
342 **observation from London Heathrow and Lakenheath airport, (d) temperature readings**
343 **at the airports in (c).**



344 In contrast, Figure 5 presents an example in summertime when the effect of temperature
345 dominates the error on the CO₂ performance, and the pressure effect is minimal ($1012.0 \pm$
346 6.82 mBar). As can be seen in Figure 5 (a) for the scaled CO₂ correction, the LCS signals
347 show daytime overestimation, which coincides with daytime temperatures well above 10 °C.
348 The effect of pressure is minimal over this period except for 2-3 August, where the scaled LCS
349 CO₂ show both daytime and nighttime dips, which is characteristic of pressure drop
350 exemplified previously in Figure 4. An improved RMSE and R² values of 4.2 ppm and 0.98
351 compared to 5 ppm and 0.86 were observed for the pressure-temperature data corrected
352 relative to simple scaled data.



353

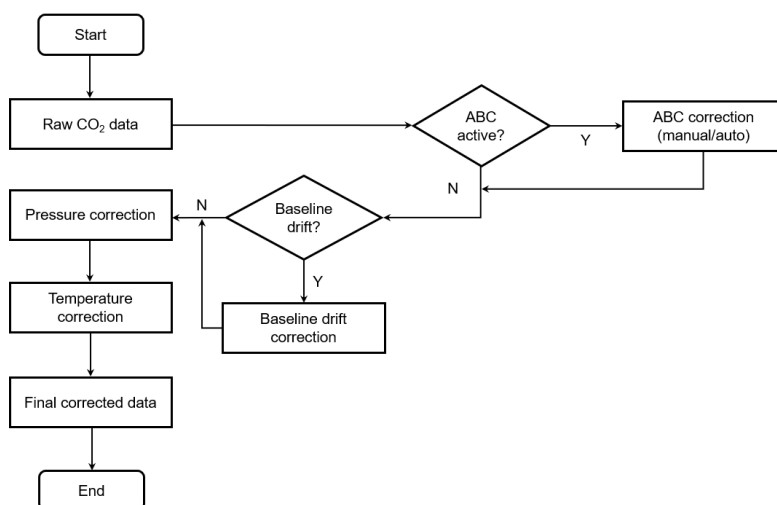
354 **Figure 5: Comparison of two correction methodologies for the period 15 July to 31**
355 **August 2023 at the urban location. (a) simple linear scaling correction, (b) combined**
356 **pressure-temperature corrected raw signal, (c) hourly pressure observation from**
357 **London Heathrow and Lakenheath airport, (d) temperature readings at the airports in**
358 **(c).**

359



360 **3.3 Framework for LCS CO₂ data processing**

361 Based on the known sources of errors discussed in section 2.4, and the results presented in
 362 3.1-3.2, the following data correction protocol (Figure 6) is proposed.



363

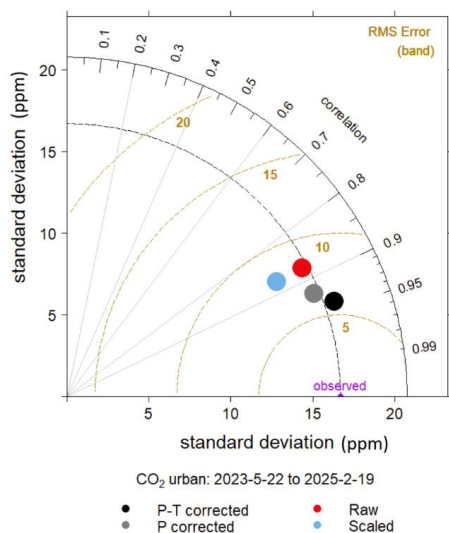
364 **Figure 6: Framework for correction of LCS CO₂ signal.**

365 This framework presents a logical approach for improving the precision and accuracy of LCS
 366 CO₂ for atmospheric application. We applied this data correction framework to evaluate the
 367 suitability of a network of CO₂ sensors in rural applications.

368 Following this framework, the performance of each data correction step—including the raw and
 369 simply scaled data relative to co-located reference measurements for the urban deployment—
 370 is summarised using a Taylor diagram (Figure 7). For the full urban dataset (Figure 7), simple
 371 scaling provides only a marginal improvement in cRMSE relative to the raw data (8.0 ppm
 372 compared with 8.2 ppm; indicated by the brown band in Figure 7), while the correlation
 373 remains unchanged ($r = 0.88$; grey radial scale in Figure 7). However, the scaling reduces
 374 signal variability (SD = 14.5 ppm) compared with the raw data (SD = 16.4 ppm) and the
 375 reference measurements (SD = 16.7 ppm; purple marker on the dashed black arc in Figure
 376 7). In contrast, the correction approaches introduced in this study result in clear improvements
 377 across all three statistics. Both the pressure-corrected and pressure-temperature-corrected
 378 datasets show reduced cRMSE (6.5 ppm), improved correlation ($r = 0.92$), and standard
 379 deviations closer to the reference data (SD = 16.3 ppm). While the pressure correction alone
 380 improves both cRMSE and correlation relative to the raw and simply scaled data, the
 381 combined pressure-temperature correction provides the closest agreement with the reference
 382 measurements.



383 Figures S2 (a) and S2 (b) present results for shorter periods in winter and summer,
 384 respectively, representing conditions dominated by pressure variability (Figure S2 (a)) and
 385 temperature variability (Figure S2 (b)) as presented in section 3.2. During the winter period, a
 386 substantial improvement is observed between the raw and pressure-corrected data, with only
 387 marginal additional improvement when temperature correction is included. This is consistent
 388 with the limited temperature variability during this period (see section 3.2). In contrast, during
 389 the summer period, when temperature variability is greater, the combined pressure-
 390 temperature correction produces a clear improvement compared with the pressure-only
 391 correction.



392

393 **Figure 7: Taylor diagram comparing raw, scaled, pressure corrected, and pressure-**
 394 **temperature corrected CO₂ measurements with co-located reference observations at**
 395 **the urban site for 22 May 2023-18 February 2025. Data points located closer to the**
 396 **reference indicate better agreement with the reference measurements. Standard**
 397 **deviations are shown as arcs of increasing radius along the x- and y-axes, Pearson**
 398 **correlation coefficients are indicated by grey radial lines extending from the origin (0**
 399 **on the y-axis to 1 on the x-axis), centred root mean square error (cRMSE) is represented**
 400 **by brown contours of increasing magnitude, referenced to the point on the x-axis.**

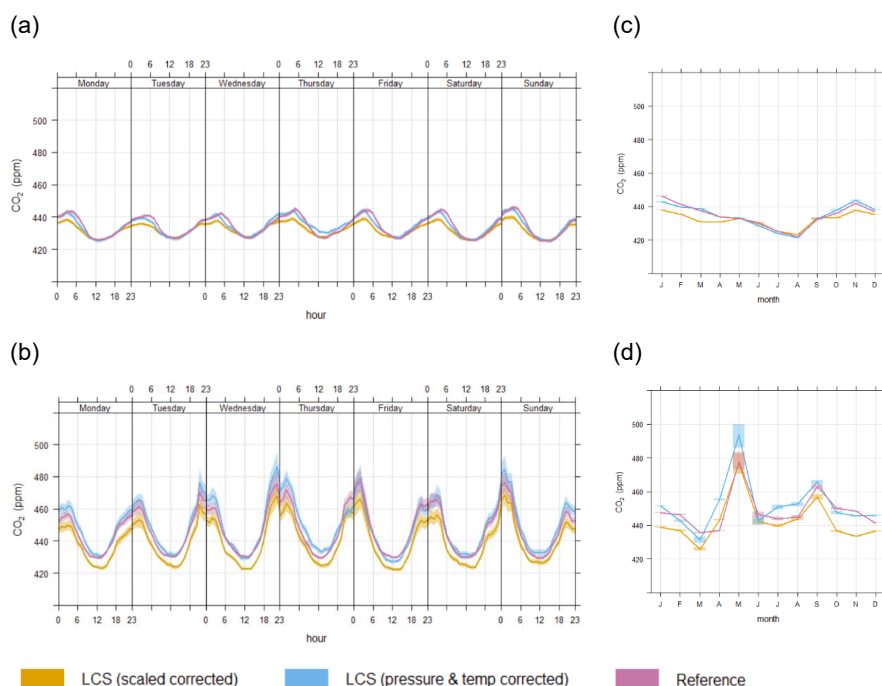
401 3.4 Suitability of LCS CO₂ in rural applications

402 3.4.1. Collocation assessment

403 To assess the potential deployment of low-cost sensor (LCS) CO₂ monitoring in rural
 404 environments, we compared measurements from corrected LCS units with those obtained



405 from reference-grade instruments at two locations, as outlined in Section 2. Although simple
 406 linear scaling produced similar trends to the reference data in both day-of-week diurnal and
 407 monthly plots, the LCS measurements consistently underestimated CO₂ concentrations,
 408 particularly during the winter months, at both urban and rural sites. However, as illustrated in
 409 Figure 8 (b-d), the LCS data corrected for pressure and temperature effects from the rural site
 410 show excellent agreement with the reference measurements, both in terms of absolute values
 411 and temporal trends.



412 **Figure 8: Comparison of rural and urban CO₂ measurements for LCS (scaled, pressure-**
 413 **temperature corrected) and reference device for the duration of the study. (a) Day-of-**
 414 **week diurnal profile at the urban site, (b) equivalent profile at the rural site, (c) monthly**
 415 **averages at the urban site, and (d) monthly averages at the rural site.**

416 3.4.2. Network assessment

417 A direct statistical comparison with the reference measurements was not performed because
 418 the reference instrument was not collocated with any of the sensors within the network.
 419 However, because the reference instrument was deployed within the same land-use
 420 environment and at a distance of less than 1 km from each sensor, the slowly varying
 421 background CO₂ signal is expected to influence both the LCS network and the reference
 422 instrument in a similar manner. Deviations from this background signal observed by individual



423 devices can therefore be attributed primarily to local sources and sinks in the immediate
424 vicinity of each measurement location. This rural deployment consequently provides a
425 valuable opportunity to assess the performance of LCS devices under rural environmental
426 conditions.

427 The observed CO₂ concentrations were strongly influenced by local emissions associated with
428 crop respiration, particularly during the night, when photosynthesis ceased and the planetary
429 boundary layer was shallower (with above background CO₂ ranging periodically in excess of
430 200 ppm for a 5-minute averaged data). Notably, daytime errors present in the uncorrected
431 dataset (Figure 9 (a) and (e)) were substantially reduced by applying the pressure-temperature
432 correction approach, as demonstrated in the comparison with the reference measurement
433 (Figure 9 (b) and (f)). In this case, the correction was primarily driven by temperature, which
434 exhibited marked diurnal variability (Figure 9 (c) and (g)), whereas pressure changes over the
435 one-month deployment period were comparatively minor (Figure 9 (d)). Figure 9 (f) shows that
436 the corrected measurements exhibit a background level comparable to that of the reference
437 data, with intermittent departures from this background. These departures, observed as short-
438 duration enhancements (for example at P11 shortly after midnight on 27 August), indicate a
439 stronger influence from nearby emission sources at this location compared with other sites
440 within the network.

441

442

443

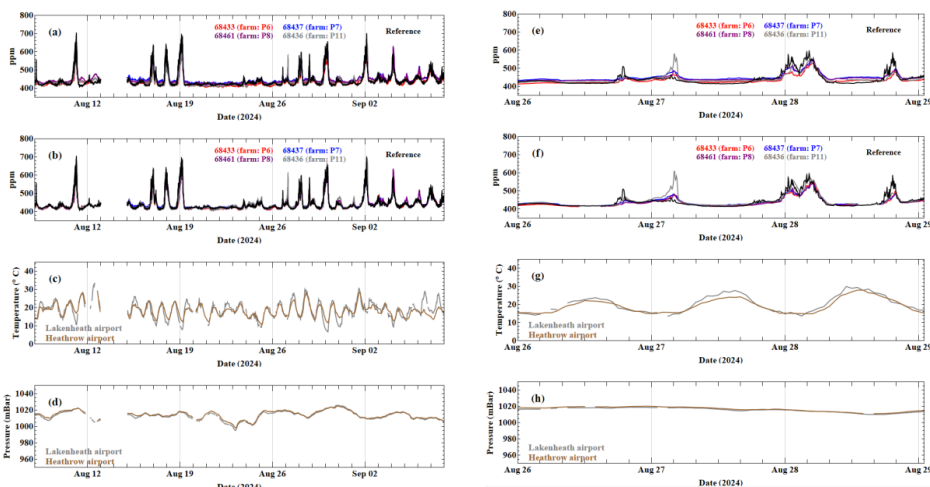
444

445

446

447

448



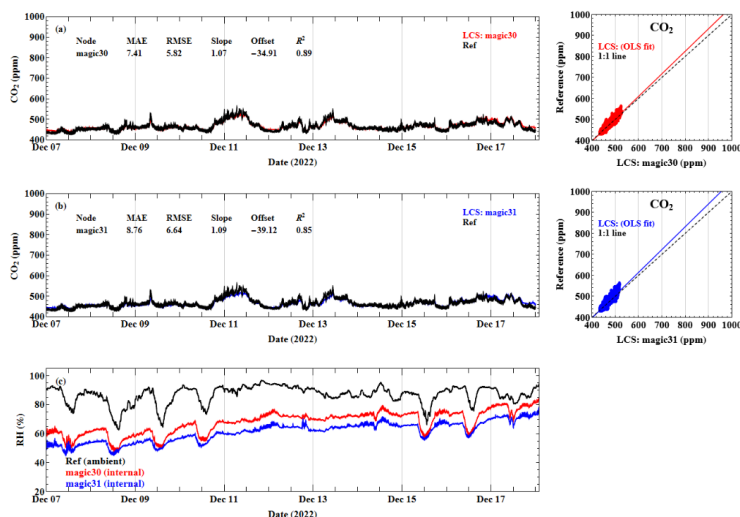
449 **Figure 9: Comparison of two correction methodologies applied to a network of four low-**
450 **cost sensor (LCS) CO₂ devices deployed at an arable farm between 8 August and 8**
451 **September 2024. Panels (a-d) show the full deployment period. (a) CO₂ concentrations**
452 **corrected using a simple linear scaling approach. (b) CO₂ concentrations derived from**
453 **the combined pressure-temperature correction applied to the raw sensor signal. (c)**
454 **hourly surface pressure observations from London Heathrow and Lakenheath airports;**
455 **and (d) corresponding air temperature observations at the airports shown in panel (c).**
456 **Panels (e-h) present zoomed composite plots of panels (a-d), respectively, for a shorter**
457 **period (26-28 August 2024), highlighting the impact of the correction methodologies on**
458 **the LCS CO₂ network data. Missing data at the beginning of the deployment are due to**
459 **cellular data transmission issues associated with the LCS network.**

460 3.5. Additional artefacts that affect performance of LCS NDIR CO₂

461 Despite all the issues discussed related to environmental effect and baseline correction, poorly
462 designed devices that utilise NDIR CO₂ sensors can still suffer from unintended artefacts
463 related to poor air circulation that presents itself as environmental effect when there is no
464 active sampling. Figure 10 shows that there was good agreement between the calibrated LCS
465 CO₂ from the Magic boxes and the reference instrument (RMSE=5-7 ppm) during the
466 deployment in the urban location, where the internal RH reading was below 80%. In contrast,
467 the results from the calibrated Magic devices (Figure 11) in the rural environment were very
468 poor (RMSE=35-61 ppm), as the unit only tracked the reference in the first 3-4 days. The
469 internal RH for box Magic boxes over these periods were generally above 75%. This effect
470 cannot be corrected empirically, as it is inherently non-systematic, unlike the temperature and
471 pressure effects described earlier. It may, however, be mitigated by ensuring adequate air

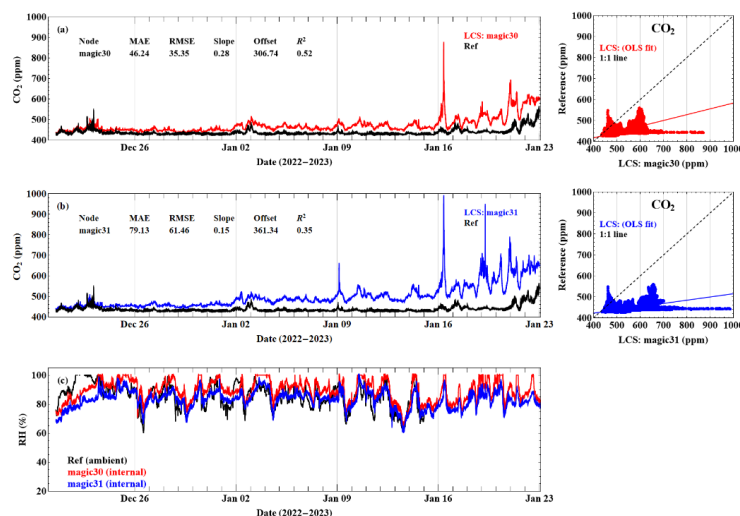


472 recirculation-such as operating the instrument within a suitably ventilated enclosure-to prevent
473 internal RH accumulation under colder conditions, or by heating the sampled air where
474 low-power operation is not a constraint.



475

476 **Figure 10: Comparison plots of a pair of LCS Magic units against the reference at the**
477 **urban location for the period 7-18 December 2022. (a) CO₂ time series with associated**
478 **validation metrics and scatter plot for Magic box 30, (b) CO₂ time series with associated**
479 **validation metrics and scatter plot for Magic box 31, and (c) RH time series comparison.**



480



481 **Figure 11: Corresponding plots to those shown in Figure 10, for the same pair of**
482 **sensors redeployed at the rural site, spanning the period from 20 December 2022 to 22**
483 **January 2023.**

484 Unlike environmental factors like temperature and RH, which can vary on a
485 microenvironmental scale (see RH readings in Figures 10 and 11), ambient pressure varies
486 on a macroenvironmental scale, as evidenced by comparing pressure readings from two
487 airports that are approximately 125 km apart (Figure S3). We used these secondary remote
488 pressure readings to correct for pressure in our study.

489 **4. Conclusions**

490 Ambient CO₂ concentrations can be effectively monitored using LCS when environmental
491 influences, particularly temperature and pressure, are appropriately accounted for. In our
492 study, pressure effects were found to dominate measurement errors under colder conditions
493 and over longer timescales associated with macro-level pressure variations. By contrast,
494 temperature effects were more pronounced in spring and summer, varying on shorter diurnal
495 timescales.

496 A notable source of measurement uncertainty in CO₂ sensors is the ABC implemented by
497 manufacturers to adjust for sensor drift. This correction often introduces step changes in
498 readings, thereby reducing both precision and accuracy (RMSE = 20ppm compared to 5 ppm
499 when this is accounted for in our study). To ensure robust data processing, we recommend
500 either disabling the ABC functionality or correcting for these step changes prior to analysis.

501 A comparison of sensor deployments in urban and rural environments demonstrates that,
502 when corrected for the dominant environmental factors identified in this work, low-cost NDIR
503 CO₂ devices are not only suitable for use in urban networks but also prove particularly valuable
504 in rural settings, where background CO₂ levels, particularly at night, are comparatively
505 elevated (as high as 700 ppm for 5-minute averaged data during the growing season). We
506 observed a relatively small diurnal variability (430-445 ppm) in the urban environment
507 compared to the rural setting (420-480 ppm). This capability enables the development of
508 innovative approaches to greenhouse gas monitoring, particularly for agriculture and land-use
509 climate impact assessments. Networks of these sensors when adequately configured and
510 characterised, when combined with modelling frameworks, provide a promising and cost-
511 effective alternative for estimating greenhouse gas fluxes in remote or otherwise under-
512 monitored locations.

513

514



515 **Competing interests:** The authors declare that they have no conflict of interest.

516

517 **Author Contributions:** OAMP and CG conceptualised the study. OAMP developed the
518 methodology. OAMP, RF, PC, RHG, LT and KL were involved in the field deployment. OAMP
519 and PC worked on data analysis. KL, LT, RF, RHG and OAMP worked on characterising the
520 devices. OAMP, PC, and CG contributed to data interpretation. OAMP prepared the
521 manuscript with contributions from all co-authors.

522

523 **Acknowledgements**

524 The authors would like to acknowledge Ross Morrison, Alexander Cumming, Brenda
525 D'Acunha (UK Centre for Ecology and Hydrology, UKCEH) for facilitating collocation at the
526 rural site, Luke Palmer (F.F. C. Palmer and Sons Stowbridge Farm Ltd) for access to the rural
527 arable site and Roderic Jones (University of Cambridge) for general discussion about the
528 project. This work was supported by the Natural Environment Research Council (UKRI NERC)
529 Changing the Environment Programme through their support for the Centre for Landscape
530 Regeneration [grant number NE/W00495X/1].

531

532

533

534

535

536

537

538

539

540

541

542

543



544 **References**

545 Arzoumanian, E., Vogel, F. R., Bastos, A., Gaynullin, B., Laurent, O., Ramonet, M., and Ciais,
546 P. (2019): Characterization of a commercial lower-cost medium-precision non-dispersive
547 infrared sensor for atmospheric CO₂ monitoring in urban areas, *Atmos. Meas. Tech.*, 12, 2665-
548 2677, <https://doi.org/10.5194/amt-12-2665-2019>.

549 Cai, Q., Zeng, N., Yang, X., Xu, C., Wang, Z., and Han, P. (2025): A 30-month field evaluation
550 of low-cost CO₂ sensors using a reference instrument, *Atmos. Meas. Tech.*, 18, 4871-4884,
551 <https://doi.org/10.5194/amt-18-4871-2025>.

552 Carslaw, D. C. and Ropkins, K. (2012): openair - An R package for air quality data analysis.
553 *Environmental Modelling and Software*, 27-28, 52-61.
554 <https://doi.org/10.1016/j.envsoft.2011.09.008>

555 Carslaw, D.: worldmet (2020): Import Surface Meteorological Data from NOAA Integrated
556 Surface Database (ISD), R package version 0.9.2, available at: [https://CRAN.R-](https://CRAN.R-project.org/package=worldmet)
557 [project.org/package=worldmet](https://CRAN.R-project.org/package=worldmet), last access: 4 April 2025.

558 Crilley, L. R., Shaw, M., Pound, R., Kramer, L. J., Price, R., Young, S., Lewis, A. C., and Pope,
559 F. D. (2018): Evaluation of a low-cost optical particle counter (Alphasense OPC-N2) for
560 ambient air monitoring, *Atmospheric Measurement Techniques*, 11, 709-720,
561 <https://doi.org/10.5194/amt-11-709-2018>.

562 Delaria, E. R., Kim, J., Fitzmaurice, H. L., Newman, C., Wooldridge, P. J., Worthington, K., and
563 Cohen, R. C. (2021): The Berkeley Environmental Air-quality and CO₂ Network: field
564 calibrations of sensor temperature dependence and assessment of network-scale CO₂
565 accuracy, *Atmos. Meas. Tech.*, 14, 5487-5500, <https://doi.org/10.5194/amt-14-5487-2021>.

566 Di Antonio, A., Popoola, O. A. M., Ouyang, B., Saffell, J., and Jones, R. L. (2018): Developing
567 a relative humidity correction for low-cost sensors measuring ambient particulate matter,
568 *Sensors*, 18, 2790, <https://doi.org/10.3390/s18092790>.

569 Dubey, R., Telles, A., Nikkel, J., Cao, C., Gewirtzman, J., Raymond, P.A., Lee, X. (2024): Low-
570 Cost CO₂ NDIR, *Sensors, Performance Evaluation and Calibration Using Machine Learning*
571 *Techniques*, 24, 5675, <https://doi.org/10.3390/s24175675>.

572 García, J., Rincón, F., Casanova-Chausson, S., Hernando, A., and Serrano, A. (2021):
573 Design and deployment of a low-cost CO₂ monitoring network for indoor and urban
574 environments, *Sensors*, 21, 1-24, <https://doi.org/10.3390/s21041533>.



- 575 Heger, A., Kleinschmidt, V., Gröngröft, A., Kutzbach, L., and Eschenbach, A. (2020):
576 Application of a low-cost NDIR sensor module for measurements of in situ soil CO₂
577 concentration, EGU General Assembly 2020, Online, 4-8 May 2020, EGU2020-5819,
578 <https://doi.org/10.5194/egusphere-egu2020-5819>.
- 579 Intergovernmental Panel on Climate Change (IPCC) (2018): Global warming of 1.5 °C: An
580 IPCC special report on the impacts of global warming of 1.5 °C above pre-industrial levels and
581 related global greenhouse gas emission pathways, IPCC, <https://www.ipcc.ch/report/sr15/>.
- 582 Jiao, W., Hagler, G., Williams, R., Sharpe, R., Brown, R., Garver, D., Judge, R., Caudill, M.,
583 Rickard, J., Davis, M., Weinstock, L., Zimmer-Dauphinee, S., and Buckley, K. (2016):
584 Community Air Sensor Network (CAIRSENSE) project: Evaluation of low-cost sensor
585 performance in a suburban environment in the southeastern United States, *Atmos. Meas.*
586 *Tech.*, 9, 5281-5292, <https://doi.org/10.5194/amt-9-5281-2016>.
- 587 LI-COR, USA. Support: LI-7815 CO₂/H₂O trace gas analyzer. URL
588 <https://www.licor.com/env/support/LI-7815/topics/specifications.html>, last access: 2
589 November 2025.
- 590 Lopez-Coto, I., Ghosh, S., Prasad, K. R., and Whetstone, J. (2017): Tower-based greenhouse
591 gas measurement network design - the National Institute of Standards and Technology North
592 East Corridor Testbed, *Adv. Atmos. Sci.*, 34, 1095-1105.
- 593 Macagga, D., Marshall, M., MacLeod, D., and van Oijen, M. (2024): Validation and field
594 application of a low-cost device to measure CO₂ and evapotranspiration fluxes, *Atmos. Meas.*
595 *Tech.*, 17, 1317-1334, <https://doi.org/10.5194/amt-17-1317-2024>.
- 596 Martin, C. R., Zeng, N., Karion, A., Dickerson, R. R., Ren, X., Turpie, B. N., and Weber, K. J.
597 (2017): Evaluation and environmental correction of ambient CO₂ measurements from a low-
598 cost NDIR sensor, *Atmos. Meas. Tech.*, 10, 2383-2395, [https://doi.org/10.5194/amt-10-2383-](https://doi.org/10.5194/amt-10-2383-2017)
599 2017.
- 600 Mead, M. I., Popoola, O. A. M., Stewart, G. B., Landshoff, P., Calleja, M., Hayes, M., Baldoví,
601 J. J., McLeod, M. W., Hodgson, T. F., Dicks, J., Lewis, A. C., Cohen, J., Baron, R., Saffell, J.
602 R., and Jones, R. L. (2013): The use of electrochemical sensors for monitoring urban air quality
603 in low-cost, high-density networks, *Atmospheric Environment*, 70, 186-203,
604 <https://doi.org/10.1016/j.atmosenv.2012.11.060>.
- 605 Miles, N. L., Davis, K. J., Richardson, S. J., Lauvaux, T., Martins, D. K., Deng, A. J., Balashov,
606 N., Gurney, K. R., Liang, J., Roest, G., Wang, J. A., and Turnbull, J. C. (2021): The influence



607 of near-field fluxes on seasonal carbon dioxide enhancements, *Carbon Balance Manag.*, 16,
608 4, <https://doi.org/10.1186/s13021-020-00166-z>.

609 Müller, M., Graf, P., Meyer, J., Pentina, A., Brunner, D., Perez-Cruz, F., Hüglin, C., and
610 Emmenegger, L. (2020): Integration and calibration of non-dispersive infrared (NDIR) CO₂
611 low-cost sensors and their operation in a sensor network covering Switzerland, *Atmos. Meas.*
612 *Tech.*, 13, 3815-3834, <https://doi.org/10.5194/amt-13-3815-2020>.

613 Pereira, P.F., Ramos, N. M. M. (2022): Low-cost Arduino-based temperature, relative humidity
614 and CO₂ sensors - An assessment of their suitability for indoor built environments, *Journal of*
615 *Building Engineering*, 60,105151, <https://doi.org/10.1016/j.jobe.2022.105151>.

616 Ren, X., Wu, K., Yang, D., Liu, Y., Wang, Y., Wang, T., Cai, Z., Yao, L., Zhao, T., Wang, J.,
617 Jiang, Z. (2025): Effects of Environmental Factors on the Performance of Ground-Based Low-
618 Cost CO₂ Sensors. *Sensors*, 25, 6114, <https://doi.org/10.3390/s25196114>.

619 Seo, Y., Kim, H., Park, S., Jeong, S., and Lee, S. (2022):
620 Field deployment of a low-cost CO₂ sensor network to characterise spatio-temporal variability
621 in an urban area, *Sensors*, 22, 1-18, <https://doi.org/10.3390/s22155675>.

622 Senseair, K33 LP T. URL <https://senseair.com/product/k33-lp-t/>, last access: 2 November
623 2025.

624 Senseair, S8. URL <https://senseair.com/product/s8/>, last access: 2 November 2025.

625 Senseair, Sunrise. URL <https://senseair.com/product/sunrise/>, last access: 2 November 2025.

626 Shusterman, A. A., Kim, J., Lieschke, K. J., Newman, C., Wooldridge, P. J., and Cohen, R. C.
627 (2018): Observing local CO₂ sources using low-cost, near-surface urban monitors, *Atmos.*
628 *Chem. Phys.*, 18, 13773-13785, <https://doi.org/10.5194/acp-18-13773-2018>.

629 Si, M., Yao, N., Li, Z.-L., Liu, X., Tang, B.-H., and Nerry, F. (2024): Feasibility of urban-rural
630 temperature difference method in surface urban heat island analysis under non-uniform rural
631 landcover: a case study in 34 major urban agglomerations in China, *Remote Sensing*, 16,
632 1232, <https://doi.org/10.3390/rs16071232>.

633 Sloan, J., Carter, E., and Smith, R. (2025): Designing CO₂ monitoring systems for agricultural
634 land using NDIR sensors for citizen scientists, *AgriEngineering*, 7, 85,
635 <https://doi.org/10.3390/agriengineering7030085>.

636 Song, J., Fan, S., Lin, W., Mottet, L., Woodward, H., Davies Wykes, M., and Linden, P. F.
637 (2018): Natural ventilation in cities: the implications of fluid mechanics, *Building Research &*
638 *Information*, 46, 809-828, <https://doi.org/10.1080/09613218.2018.1468158>.



- 639 Spinelle, L. Gerboles, M., Villani, M.G., Aleixandre, M., Bonavitacola, F. (2017): Field
640 calibration of a cluster of low-cost commercially available sensors for air quality monitoring.
641 Part B: NO, CO and CO₂, *Sensors and Actuators B: Chemical*, 238, 706-715,
642 <https://doi.org/10.1016/j.snb.2016.07.036>.
- 643 Turner, A. J., Shusterman, A. A., McDonald, B. C., Teige, V., Harley, R. A., and Cohen, R. C.
644 (2016): Network design for quantifying urban CO₂ emissions: assessing trade-offs between
645 precision and network density, *Atmos. Chem. Phys.*, 16, 13465-13475,
646 <https://doi.org/10.5194/acp-16-13465-2016>.
- 647 Weng, Q., Lu, D., and Schubring, J. (2004): Estimation of land surface temperature-vegetation
648 abundance relationship for urban heat island studies, *Remote Sensing of Environment*, 89,
649 467-483, <https://doi.org/10.1016/j.rse.2003.11.005>.
- 650 World Meteorological Organization (WMO) (2023):
651 Integrating Low-Cost Sensor Systems and Networks to Enhance Air Quality Applications,
652 WMO-No. 1307, World Meteorological Organization, Geneva, Switzerland.
- 653 Wu, L., Broquet, G., Ciais, P., Bellassen, V., Vogel, F., Chevallier, F., Xueref-Remy, I., and
654 Wang, Y. (2016): What would dense atmospheric observation networks bring to the
655 quantification of city CO₂ emissions?, *Atmos. Chem. Phys.*, 16, 7743-7771,
656 <https://doi.org/10.5194/acp-16-7743-2016>.
- 657 Wu, X., Maurer, C., Stutz, J., and Bard, J. (2019):
658 Evaluation and calibration of low-cost sensors for measuring ambient CO₂ in an urban
659 environment, *Atmos. Meas. Tech.*, 12, 6401-6415, <https://doi.org/10.5194/amt-12-6401-2019>.
- 660 Wu, Z., Pang, X., Xing, B., Shang, Q., Wu, H., Lu, Y., Wu, H., Lyu, Y., Li, J., Wang, B., Ding,
661 S., Chen, D., Chen, J. (2023): Development of a Portable and Sensitive CO₂ Measurement
662 Device with NDIR Sensor Clusters and Minimizing Water Vapor Impact. *Sustainability*, 15,
663 1533, <https://doi.org/10.3390/su15021533>.
- 664 Xu, M., Xu, Y., Tao, J., Wen, L., Zheng, C., Yu, Z., He, S. (2024): Development of a compact
665 NDIR CO₂ gas sensor for harsh environments, *Infrared Physics & Technology*, 136, 105035,
666 <https://doi.org/10.1016/j.infrared.2023.105035>.
- 667 Yang, Y., Zhou, M., Wang, T., Yao, B., Han, P., Ji, D., Zhou, W., Sun, Y., Wang, G., and Wang,
668 P. (2021): Spatial and temporal variations of CO₂ mole fractions observed at Beijing, Xianghe,
669 and Xinglong in North China, *Atmos. Chem. Phys.*, 21, 11741-11757,
670 <https://doi.org/10.5194/acp-21-11741-2021>.